Superalloys 2012: 12th International Symposium on Superalloys
Edited by: Eric S. Huron, Roger C. Reed, Mark C. Hardy, Michael J. Mills, Rick E. Montero, Pedro D. Portella, Jack Telesman
TMS (The Minerals, Metals & Materials Society), 2012

NANOINDENTATION AND NANO-COMPRESSION TESTING OF Ni_3Al PRECIPITATES

B. Gan[1], H. Murakami[2], R. Maaß[3], L. Meza[3], J.R. Greer[3], T. Ohmura[2], S. Tin[1]
[1]Illinois Institute of Technology, 10 W. 32nd St., Chicago, IL 60616, U.S.A
[2]National Institute for Materials Science, Tsukuba Science City, Ibaraki 305-0047, Japan
[3]California Institute of Technology, Division of Engineering and Applied Science, 1200 E. Colorado Blvd., Pasadena, CA 91125, U.S.A

Keywords: superalloy, γ' precipitate, nanoindentation, nano-compression

Abstract

Using an AFM-based instrumented nanoindentation system, the nanoindentation response of γ' particles (Ni_3Al) in a Ni-base single crystal superalloy CMSX-4 was characterized to demonstrate the influence of the softer γ matrix on the measurement of nano-mechanical properties of γ' particles. The properties of the γ' particles were measured after both a standard and a coarsening heat treatment, in which the initially sub-micron sized cuboidal γ' particles transformed to large, irregularly shaped γ' precipitates with dimensions in excess of 30 μm. The measured nano-hardness of the coarsened γ' precipitates in CMSX-4 appears to increase slightly with the increasing load. Nano-compression testing of cuboidal γ' particles, electrolytically extracted from a CMSX-4 after a standard solution and age heat treatment, was also performed. With a maximum value of 10 GPa, the measured yield stress of these dislocation-free γ' particles approaches the ideal strength and is equivalent to ~G/17. Compared to the measured yield strengths of γ' phase in its bulk crystal form, these nano-compression results are more than a factor of 33 higher. Additionally, the 'softening' effect of Ga^+ ion implantation on the strength of dislocation-free nanocrystals was also assessed. The resulting yield strengths of cuboidal γ' precipitates imaged with a focused ion beam were at least 5 GPa lower than those that had not been subjected to Ga^+ ion implantation.

Introduction

Ni-base single crystal superalloys are commonly used for gas turbine blades of aero engine and power generation system, as they possess an extraordinary combination of excellent high temperature mechanical properties, a long term structural integrity and microstructural stability, and robustness to surface degradation in highly corrosive and oxidizing environment [1-3]. The underlying microstructure of this class of materials consists of a continuous disordered FCC γ matrix, strengthened by ordered $L1_2$ intermetallic γ' precipitates [4]. Success in the new alloy development programs that utilize integrated computational materials modeling approaches [5] and novel characterization tools [6-8] relies heavily on our understanding of the fundamental mechanisms governing the mechanical behavior and a detailed characterization of the constitutive properties of individual phases.

Assessment of the mechanical response of the constituent phases in their bulk crystal form may provide insight into the deformation mechanisms of the two phase structure of Ni-base superalloys [9]. However, micro-compression tests of Ni micro-pillars [10] and nano-compression tests of Au nano-pillars [11] clearly demonstrated that the single crystal metallic micro- and nano-structures considerably outperform their macroscopic counterparts in strength. Consequently, in order to have a more precise measurement of the constitutive properties of the individual constituent phases of Ni-base superalloys, *in-situ* characterization tools are needed to directly probe their mechanical responses. In the current study, nanoindentation measurement of the constituent phases of a Ni-base superalloy was compared to results from the nano-compression testing of freestanding cuboidal γ' particles to assess the influence of sample sizes on mechanical properties. Additionally, the effect of the Ga^+ ion implantation on the nanoscale mechanical properties was also assessed.

Experimental Materials and Procedures

CMSX-4 superalloy is a second generation single crystal Ni-base superalloy. Single crystal samples of CMSX-4, with a nominal chemistry of Ni–6.5Cr–9.0Co–0.6Mo–3.0Re–6.0W–5.6Al–1.0Ti–6.5Ta–0.1Hf (wt.%), were subjected to the standard three-step heat treatment process that consisted of a solution heat treatment at 1320˚C for 2 h, followed by a primary age at 1140˚C for 6 h and a secondary age at 870˚C for 16 h [12]. Following this heat treatment, the microstructure of the 'standard' CMSX-4 consisted of a uni-modal distribution of cuboidal γ' particles with coherent interfaces and edge lengths varying between 300 nm and 500 nm [12]. For this alloy, the magnitude of the lattice misfit between the γ and γ' phases, defined as $2(a_{\gamma'}-a_{\gamma})/(a_{\gamma'}+a_{\gamma})$, has been reported to be $(1.0\pm0.5)\times10^{-3}$ within the interdendritic region and $(-4.5\pm0.5)\times10^{-3}$ within the dendritic core at room temperature [13].

Nanoindentation of constituent phases of CMSX-4

To induce the formation of semi-coherent, coarsened γ' precipitates, CMSX-4 samples with the standard heat treatment condition were first compressed at room temperature to an engineering strain of 5% and then sealed into an argon purged quartz tube and annealed at 1275˚C for 120 h to partially solutionize and coarsen the γ' precipitates. This was followed by a heat treatment at 1140˚C for 6 h and then at 870˚C for 16 h, before being quenched in water. These samples are referred to as the 'coarsened' CMSX-4. All of the specimens were metallurgically prepared using standard techniques and care was taken to minimize the influence of residual stresses and plastic deformation along the sample surface. Using extremely low loads, the samples were finished with a final polish using 0.02 μm colloidal silica. Electro-polishing techniques were not used, as preferential etching of the γ and γ' phases will occur and result in surface topology differences. Microstructural characterization was conducted using a JSM-7001F SEM.

A Hysitron SPM-3800 Atomic Force Microscope (AFM) with a pyramidal-shape Berkovich diamond indenter was used to perform the nanoindentation measurements of the individual phases. The tip radius was measured to be 200 nm. Prior to indentation tests of CMSX-4, the system compliance and area function of the indenter were calibrated by measuring the

characteristic load–depth curves of fused silica. The surface profile of the CMSX-4 samples was scanned to verify that the sample tilt was less than 0.3˚ and the height difference between γ and γ' phases was less than 3 nm. With the scanned surface topography, sites of interest were selected for the indentation tests. Prior to each indentation test, a drift correction procedure was conducted. For the 'standard' CMSX-4, the peak load changed from 250 μN to 500 μN; while for the 'coarsened' CMSX-4, the peak loads varied from 250 μN to 1000 μN. The loading and unloading rates were 25 μN for all cases. The dwell time at the maximum load was 10 s. To minimize the effect of strain gradients between different indents, the spacing between discrete indents was always selected to be greater than 1 μm.

Nano-compression of freestanding γ' particles

TEM foils of the 'standard' CMSX-4 specimen were prepared by conventional twin-jet electro-polishing in a solution of 68% methanol, 10% perchloric acid, 9% distilled water, and 13% Butyl cellosolve by volume. The optimum polishing condition was determined to be -35˚C with a voltage of 20 V. These foils were investigated via transmission electron microscopy (TEM, Tecnai TF20, double tilt holder, 200 kV) to confirm that the γ' precipitates were largely dislocation-free.

Disks with a diameter of 5 mm and a thickness of 2 mm were cut out from the 'standard' CMSX-4 specimen. These disks were electrochemically etched in an aqueous electrolyte (H_3PO_4: Methanol=1:2) with a voltage of 6 V, so that the γ matrix was selectively etched away and the γ' precipitates could be extracted. A centrifuge was used to separate the γ' precipitates from the electrolyte. The γ' particles were stored in an ethanol solution. To isolate individual particles for nano-compression tests, a droplet of the ethanol solution containing γ' particles was placed on a chemically cleaned Si wafer and then the ethanol was allowed to evaporate. Although most particles were observed to form clusters, some isolated, freestanding γ' particles could be easily identified. Such γ' particles are largely dislocation-free and possess plane normals that are oriented along the <100> directions [3]. Individual γ' particles with parallel top and bottom surfaces were carefully selected for the uniaxial nano-compression tests along their longest axis. One set of electrolytically extracted γ' particles was imaged with a single ion rastering scan in a Focused Ion Beam (FIB), using 30 kV acceleration voltage, 30 pA current and a magnification of 6000×. A direct comparison of the measured properties associated with the electrolytically extracted and ion-imaged γ' particles was made to understand the effect of Ga^+ ion implantation on the underlying deformation mechanisms.

In-situ nano-compression tests of these freestanding γ' particles were performed in the SEMentor, an *in-situ* nanomechanical instrument comprised of the Dynamic Contact Module (DCM) that is similar to a Nanoindenter (Agilent Corp.) but inside of a field-emission SEM (FEI Quanta 200). The nominal strain rate was 1×10^{-3} s^{-1}. *Ex-situ* nano-compression tests with a constant displacement rate of 2 nm/s was also conducted with a Hysitron Triboscope Nanoindenter, equipped with an 8 μm-diameter flat-punch diamond indenter serving as the compression anvil. The deformed morphology and surface topography of electrolytically-extracted and ion-imaged γ' particles were observed using the SEM and the tapping-mode of AFM, respectively.

Experimental Results

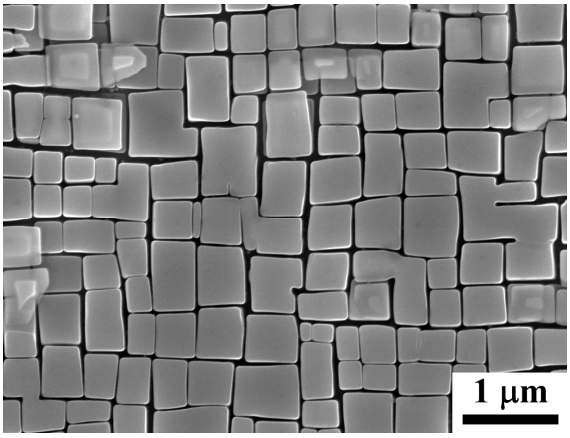

Figure 1. A SEM micrograph revealing the microstructure of the 'standard' CMSX-4; cuboidal and tetragonal γ' particles coherently dispersed in the γ matrix.

Figure 1 shows a SEM micrograph of the microstructure of the 'standard' CMSX-4 following the standard heat treatment. Microstructural characterization of these specimens reveals that cuboidal and tetragonal γ' particles were coherently dispersed in the γ matrix with an average edge length of 450 nm.

To induce the formation of large γ' particles in CMSX-4, a cellular recrystallization transformation was utilized. Room temperature deformation followed by the high temperature annealing results in the formation of a high angle grain boundary that sweeps through two phase γ/γ' microstructure to minimize the dislocation density and stored strain energy. Trailing immediately behind the mobile high angle boundary is a cellular precipitation reaction in which γ and γ' phases reform as lamellar structures to restore the equilibrium volume fraction of the constituent phases. Due to the enhanced kinetics associated with diffusion along the mobile boundary, the sizes of the phases that form during this cellular recrystallization reaction tend to be significantly larger than the original morphologies.

Figure 2 shows a SEM micrograph of the microstructure of the 'coarsened' CMSX-4 after an electrochemically etching in the aqueous electrolyte (H_3PO_4: Methanol=1:2) with a voltage of 6 V. This top view of the interface between the recrystallized and the un-recrystallized regions show that the γ' precipitates coarsened in the recrystallized region; while the γ' precipitates in the un-recrystallized regions retained their coherency with the γ matrix with relatively unchanged sizes. For γ' precipitates located within the recrystallized region as well as the interdendritic regions of the 'coarsened' CMSX-4, irregularly shaped morphologies with sizes varying from 500 nm to 30 μm were observed. Large spacings between the γ' phases in the 'coarsened' CMSX-4 also led to the formation of nano-sized dispersions of γ' particles within the γ matrix. Since the solubility of γ' forming elements in the γ phase decreases as a function of temperature, precipitation of nano-sized γ' particles at the ageing temperature alleviates the degrees of super-saturation in the γ phase.

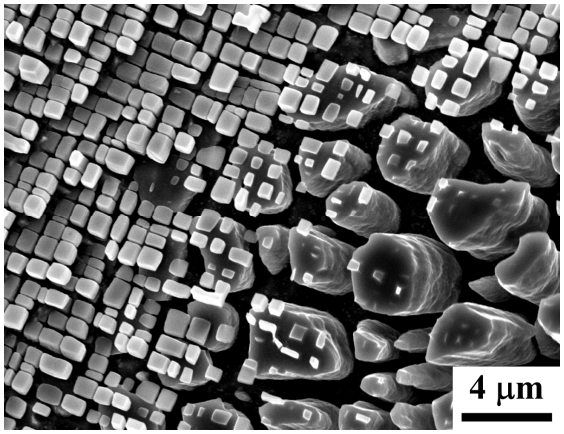

Figure 2. A SEM micrograph depicting the microstructure of the 'coarsened' CMSX-4; γ' precipitates located within the cellularly recrystallized regions preferentially coarsened, while γ' precipitates within the un-recrystallized region had a subtle change in sizes and remained coherent with the γ matrix.

Nanoindentation of constituent phases of CMSX-4

Prior to the nanoindentation measurement of the constituent phases of the 'standard' CMSX-4 following the standard heat treatment, the surface topography was scanned by the diamond tip. With the scanned image, the center of a γ' particle was selected for the indentation tests. To ensure the reproducibility of the reported results, at least 30 discrete γ' particles were measured. Representative load-depth curves of the indents made on the γ' particles of the 'standard' CMSX-4 are plotted in Figure 3, with the inserted AFM image showing one representative indent. With an onset load of ~70 μN, the 'pop-in' behavior, the sudden displacement burst following the initial elastic Hertzian contact, was observed in all of the tests. This 'pop-in' in the load depth curves can be attributed to the nucleation of dislocations in the plastically deformed region directly underneath the indenter [14].

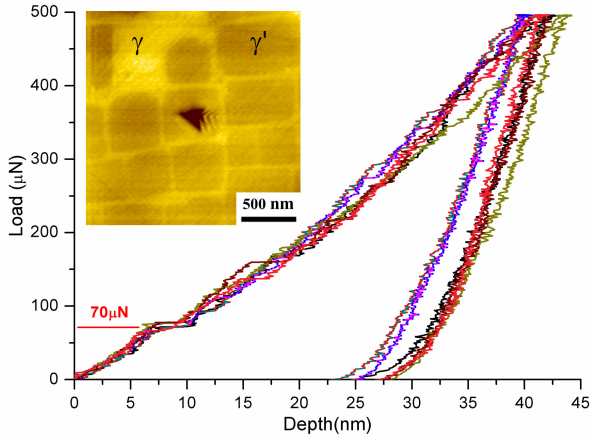

Figure 3. The load-depth curves of indents made in the γ' precipitates of the 'standard' CMSX-4. The inserted AFM image shows the indent in a γ' precipitate, tested at 500 μN load.

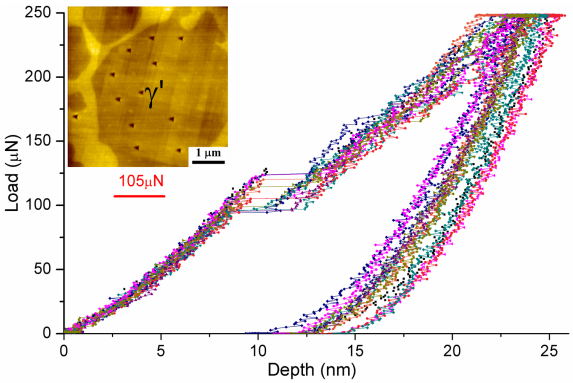

Figure 4. The load-depth curves of indents made in a coarsened γ' precipitate of the 'coarsened' CMSX-4 with a load of 250 μN. The inserted AFM image shows the corresponding indents.

Representative load-depth curves of the indents made in a coarsened γ' particle of the 'coarsened' CMSX-4 with a load of 250 μN are plotted in Figure 4, with the inserted AFM image showing the corresponding indents. The 'pop-in' behavior was observed in all of these tests. Indentation measurements were also made in regions of the sample corresponding to the single phase γ matrix. Interestingly, the onset load associated with the 'pop-in' of coarsened γ' particles, 105 μN, was noted to be higher than that of γ matrix, 75 μN. Although this is consistent with γ' phase's comparatively higher resistance to plastic deformation, the 'pop-in' load for the coarsened γ matrix is nominally same to that determined for the γ' particles in the 'standard' CMSX-4 samples.

Representative load-depth curves of indents made in a coarsened γ' particle of the 'coarsened' CMSX-4 with a size of 8 μm, tested at loads of 250 μN, 500 μN and 1000 μN are shown in Figure 5, with the inserted AFM image showing the corresponding indents. To ensure the reproducibility, a minimum of five indents were made on the same coarsened precipitate for each load. Moreover, the indentation measurements, performed on five distinct coarsened precipitates within the sample, were nominally similar.

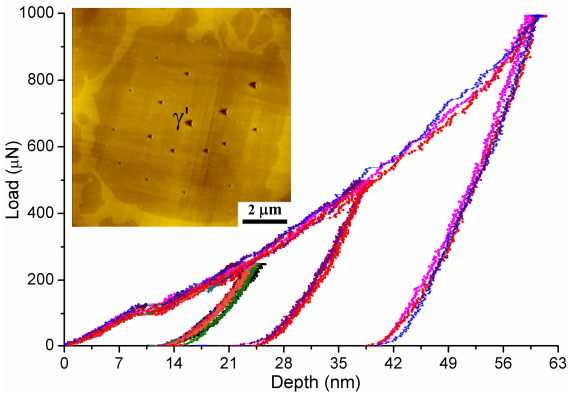

Figure 5. The load-depth curves of indents made in an 8 μm sized coarsened γ' precipitate, tested at a load of 250 μN, 500 μN and 1000 μN. The corresponding indents are shown in the inserted AFM image.

As seen in Figure 5, the 'pop-in' behavior was observed in all of the tests and did not vary as a function of the indentation load. Both the load associated with the onset and the relative displacement of the 'pop-in' events was found to be nominally similar for all of the tests. Superposition of discrete load-depth curves for different places not only indicates a good reproducibility of test, but also suggests that the measured nano-hardness trend is not significantly affected by the presence of minor composition gradients in the coarsened γ' precipitates or the influence of the surrounding γ matrix. The convergence of the loading segments for the various load-depth curves suggests that the nucleation and multiplication process of dislocations in the plastically deforming region under the indenter is roughly similar, even though the onset load of the 'pop-in' varies slightly.

The measured hardness and Young's modulus of the coarsened γ' precipitates were characterized as a function of indentation loads and the average results are summarized in Figure 6. As seen in Figure 6, the measured Young's modulus does not vary as a function of the indentation load. On the other hand, the measured hardness of the coarsened γ' precipitates of the 'coarsened' CMSX-4 appears to increase slightly with increasing load. Due to the physically large size of the coarsened γ' precipitates, compared with the indent sizes, the influence of the surrounding softer γ matrix can be minimized. Since the coarsened γ' precipitates have an intrinsically low dislocation density [15], their influence on the observed experimental results is unlikely. Hence, the observed increase in hardness as a function of load may be attributed to the increase in the density of geometrically necessary dislocations [16] that form within the plastic volume underneath the indenter.

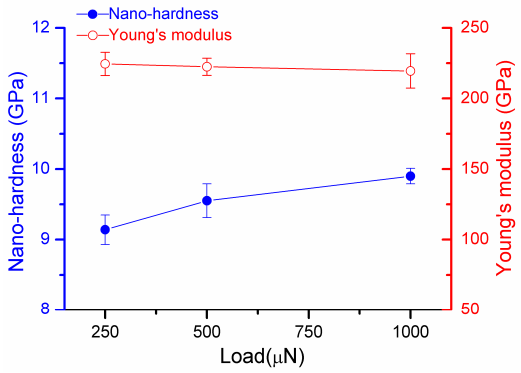

Figure 6. Variation of the measured nano-hardness and Young's modulus as a function of the indentation load.

Nano-compression of freestanding γ' particles

In addition to indirectly assessing the micro-mechanical properties of γ' precipitates in the 'standard' CMSX-4 by measuring the nanoindentation response of coarsened γ' precipitates in the 'coarsened' CMSX-4, their constitutive properties could also be directly evaluated via the nano-compression tests of freestanding γ' particles along the ⟨100⟩ direction.

A bright field TEM image of the 'standard' CMSX-4 is depicted in Figure 7(a) and shows the presence of several bending contours. The observation that no dislocation lines were

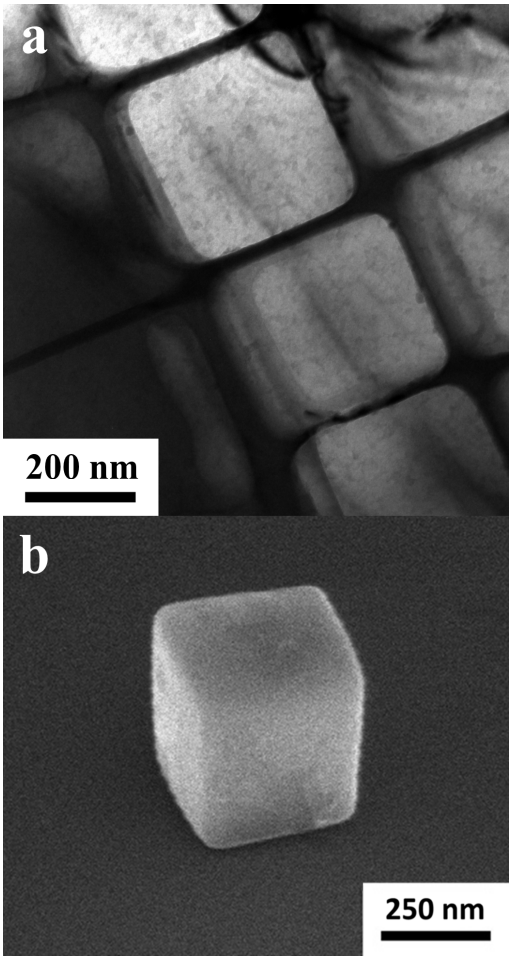

Figure 7: (a) A bright-field TEM image of the 'standard' CMSX-4 and this confirms that γ' particles are largely dislocation-free. (b) A SEM image of a freestanding γ' particle, rested on a Si wafer.

identifiable in the γ' precipitates of CMSX-4 superalloy following a standard heat treatment is in agreement with published literature on Ni-base superalloys [8, 17]. Figure 7(b) exhibits a SEM image of a freestanding γ' particle, resting on a Si wafer and possessing plane normals that are oriented along the <100> directions.

Figure 8 exhibits the flat-end diamond indenter and a side view of a dislocation-free, freestanding γ' particle with parallel top and bottom surfaces. The inserted image shows the corresponding γ' particle after deformation that has a pancake shape. For compression testing at such a small scale, alignment is a very critical issue, as misalignment will result in a stress concentration that leads to an imprecise measurement. *In-situ* nano-compression instrument enables us to test carefully selected γ' particles along their longest axis, ensuring a good alignment. The high sensitivity of load and displacement was fully exploited to assess their mechanical response in a quantitative manner. With the SEM micrograph of their top view, the original area of the top surface of the γ' particles was measured to calculate the engineering stress.

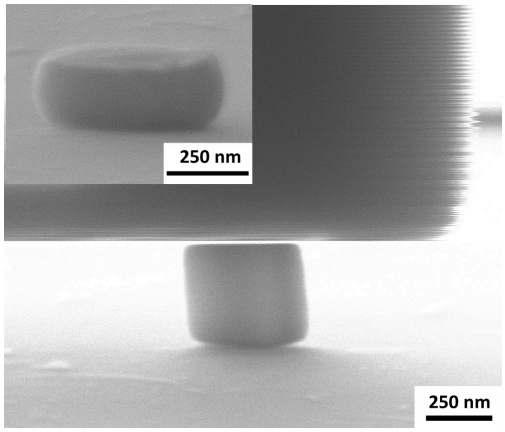

Figure 8. A SEM image of the indenter, the side view of a dislocation-free γ' particle, with the inserted image showing the dislocation-free γ' particle after deformation.

Figure 9(a) shows the engineering stress-displacement of electrolytically extracted γ' particles. The curves exhibiting a controlled unload and marked with an arrow were obtained during the *in-situ* tests inside the SEM, while the rest of the curves were generated during the *ex-situ* tests using the Hysitron Triboscope Nanoindenter. Deformation of these dislocation-free γ' particles reveals an initial elastic response, followed by the occurrence of a catastrophic instability, in which the nanoindenter was unable to maintain the prescribed displacement rate. In all of the tests, no work hardening was observed and the maximum strength of the sample corresponds to the yield strength or stress at which the plastic instability first occurs. Similar behavior has been observed during the *in-situ* nano-compression tests of such freestanding γ' particles inside the SEM [18], which is less quantitative due to the insufficient precision in measuring the stress and strain; as well as *in-situ* nano-compression tests of freestanding γ' particles inside the TEM [19].

To ensure the reproducibility of the reported results, a minimum of 20 tests were conducted to get the average results. Despite the significant scatter in the yield stress (4.6±2.7 GPa), it is interesting to note that the maximum measured axial stress along the [001]-axis is in excess of 10 GPa, which corresponds to a resolved shear stress of 4.2 GPa, when a {111}⟨110⟩ slip system is assumed. This value represents ~37% of the theoretical resolved shear strength (11.2 GPa).

Figure 9(b) shows the engineering stress-displacement of the ion-imaged γ' particles, where the y-axis scale is identical to the curves plotted in Figure 9(a) for comparison. It is clearly evident that ion-imaged samples exhibit lower yield stresses, defined as the first resolvable displacement burst longer than ~0.6 nm. 11 tests were conducted and the measured yield stresses varied from 1.0 GPa to 5.5 GPa. Similar to the electrolytically extracted γ' particles, the initial loading slope also has a significant variation.

Moreover, a clear distinction in the flow response between the as-extracted and ion-imaged γ' particles was observed in Figure 9(a) and 9(b). The as-extracted γ' precipitates are dislocation-free and exhibit a single catastrophic event with a structural collapse; while

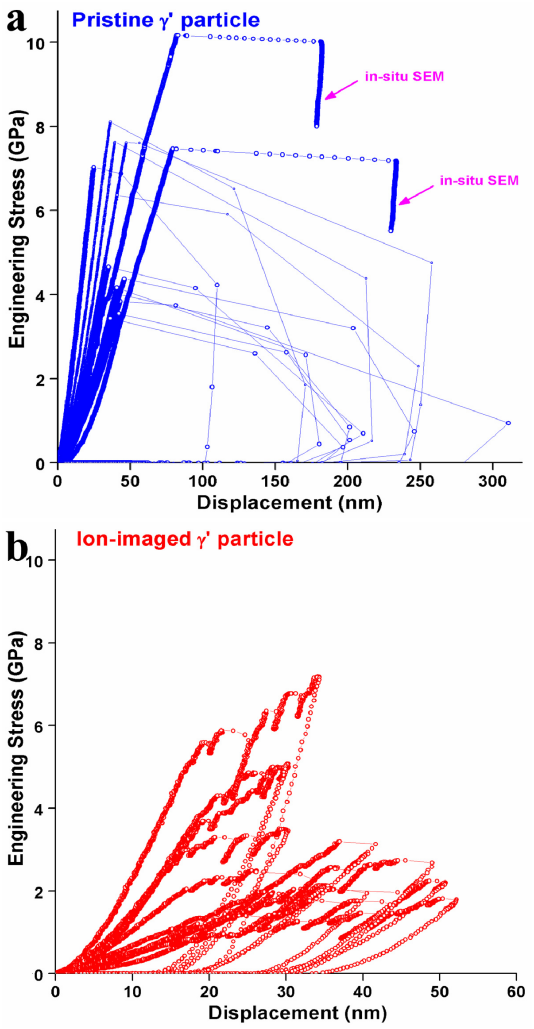

Figure 9: (a) Stress-displacement curves of the dislocation-free γ' particles and curves displaying a controlled unloading are from *in-situ* SEM tests; (b) Stress-displacement curves of the ion-imaged γ' particles.

the ion-imaged particles show an intermittent stress-displacement response after yielding. These observations are in agreement with those published results on the dislocation-free, pre-strained and FIB-milled BCC Mo-alloy with sub-micron sizes [20, 21].

Discussion

Nanoindentation of constituent phases of CMSX-4

For the AFM-based nanoindentation system, the surface of the well-polished specimen was scanned by a diamond tip. Using the scanned surface topography, sites of interest can be selected and then indented with the same tip [22]. This technique has already been used to quantify the micro-mechanical properties of individual phases of Ni-base single crystal superalloys [23-25]. However, to ensure the measured results by such techniques are

truly representative of their constitutive properties, the indentation process is revisited here. During indentation, various sources will contribute to the scatter in the testing results and these sources can be classified either as being extrinsic or intrinsic. Extrinsic sources may come from the surface condition of prepared specimens and the calibration of nanoindentation equipments. Intrinsic sources, on the other hand, may originate from the two-phase microstructure of this class of materials. The cuboidal intermetallic γ' precipitates in the 'standard' CMSX-4 specimen typically possess cube lengths of ~450 nm with inter-particle spacings of approximately 70 nm. In addition, for a well-polished specimen, without a cross-sectional view, it is difficult to know the embedded depth of the phases that are being subjected to indentation. Statistically speaking, typical dimensions of an indented γ' particle will be 450 nm by 450 nm by 225 nm. Thus, these particles can be approximated as thin films, where the maximum depth that can be imposed during indentation is approximately one-tenth of the thickness (22.5 nm). These conditions will confine the plastic deformation zone underneath the indentation entirely within the constituent phase and minimize its interaction with the interface between γ and γ' phases. However, the influence of the internal stress, induced by the lattice misfit between coherent γ and γ' phases, and the effect of γ matrix on the system compliance is still difficult to quantify. Such variables may lead to an imprecise measurement of the micro-mechanical properties of the individual γ and γ' phases in the 'standard' CMSX-4 containing sub-micron sized γ' particles.

The measured hardness and Young's modulus of the individual phases in the 'standard' and 'coarsened' CMSX-4 are summarized in Table I. For the 'coarsened' CMSX-4, the hardness of the coarsened γ' particles is higher than that of the γ matrix. Fitting the data of the segments before the occurrence of the 'pop-in' behavior with the Hertz equation reveals a consistent trend in hardness values. For the 'coarsened' CMSX-4, the hardness of the small γ' particles is in between the measured value of the coarsened γ' particles and the coarsened γ matrix, this suggests that there is an influence of the surrounding softer γ matrix on the measured properties of the small γ' precipitates. During the heat treatment to form a coarsened γ' structure, the width of the γ channel also increases. Ultimately, this results in a super-saturation of solute in these widened γ channels. Upon cooling to room temperature, nano-sized precipitates formed in the γ channels. Due to the presence of nano-sized γ' precipitates, the indentation response of the γ matrix of 'coarsened' CMSX-4 may not truly reflect the constitutive properties of the γ matrix of the 'standard' CMSX-4 specimen. These nano-sized γ' particles, potent precipitation strengtheners that are absent in the γ matrix of the 'standard' CMSX-4, increases the hardness of the γ matrix in the 'coarsened' CMSX-4 sample. As the chemistry and dislocation substructure of the γ' particles in the 'standard' CMSX-4 and the 'coarsened' CMSX-4 are nearly identical, their indentation response should be the same. However, the measured nano-hardness of the γ' particles in the 'standard' CMSX-4 is 8.5 GPa, which is lower than that of the coarsened γ' particles in the 'coarsened' CMSX-4, 9.5 GPa. This is consistent with the above observation that the soft γ matrix will affect the measurement of the individual properties of γ' particles. The effect is stronger, as the effect is stronger, as the γ matrix in the 'standard' CMSX-4 is softer than the coarsened γ matrix of the 'coarsened' CMSX-4.

Table I. Indentation results of the precipitates and matrix of 'standard' CMSX-4 and 'coarsened' CMSX-4 tested at 500 μN.

	H /GPa	Standard Deviation	E /GPa	Standard Deviation
cuboidal γ'	8.5	*0.7*	210.3	*11.2*
small γ'	9.1	*0.4*	204.7	*13.7*
Coarsened γ'	9.5	*0.6*	218.5	*7.8*
Coarsened γ matrix	8.6	*0.4*	207.0	*6.9*

As shown in Figure 6, the measured hardness of the coarsened γ' precipitates of the 'coarsened' CMSX-4 appears to increase slightly with the increasing load. This result is opposite to the decreasing trend between measured hardness and depth reported in [23, 25]. The current results suggest that such a significant decrease in hardness with the increase in depth is very likely due to the influence of the softer surrounding γ matrix. As the load increases, the plastic deformation volume underneath the indenter may encompass the γ matrix, resulting in a lower hardness value.

Nano-compression of freestanding γ' particles

Figure 10(a) and 10(b) show the representative morphology and surface topography of the electrolytically extracted γ' particles after the deformation, observed by the SEM and AFM, respectively. As shown by the inserted image in Figure 8 and Figure 10(a), the as-extracted, dislocations free γ' particle structurally collapsed into a flat pancake shape. This corresponds to a significant change in dimensions and is consistent with the large strain burst depicted in Figure 9(a). These finding are similar to the earlier work investigating the compressive response of pristine Mo-alloy BCC sub-micron sized crystals and a recent work on pristine Au nanoparticles [20, 26].

Upon reaching a high critical stress that is close to the theoretical stress, temporally correlated and explosive dislocation nucleation occurs throughout the entire nanocrystal. As no effective barriers are present to impede their motions, the nucleated dislocations run out of the nanocrystals with a high velocity. As a result, the sample undergoes a significant change in dimensions and a multitude of slip lines is present on the deformed surface of the dislocation-free γ' particles, shown in Figure 10(a) and 10(b). This is consistent with the study showing that mobile dislocations traveling on slip planes inside the nanocrystals have a much higher probability of annihilating at the free surface rather than reacting with one another at the intersecting slip planes to form a lock [27]. The presence of slip lines with various slip orientations suggests that numerous slip systems were activated concurrently, clearly corroborating that the rather homogeneous deformation of the dislocation-free γ' particles is mediated by collective motion of dislocations. This deformation behavior is different from the brittle fracture of Cu whiskers during the tensile tests [28-30].

Figure 10(c) shows a SEM image of an ion-imaged γ' particle after the deformation. The deformed morphology is consistent with the intermittent stress-displacement behavior, depicted in Figure 9(b). The presence of a few resolvable slip lines, indicated by the arrows, suggests that the ion-imaged particles respond to the applied stress by the initiation of local deformation at stress concentration and defects, induced by the Ga^+ ion implantation.

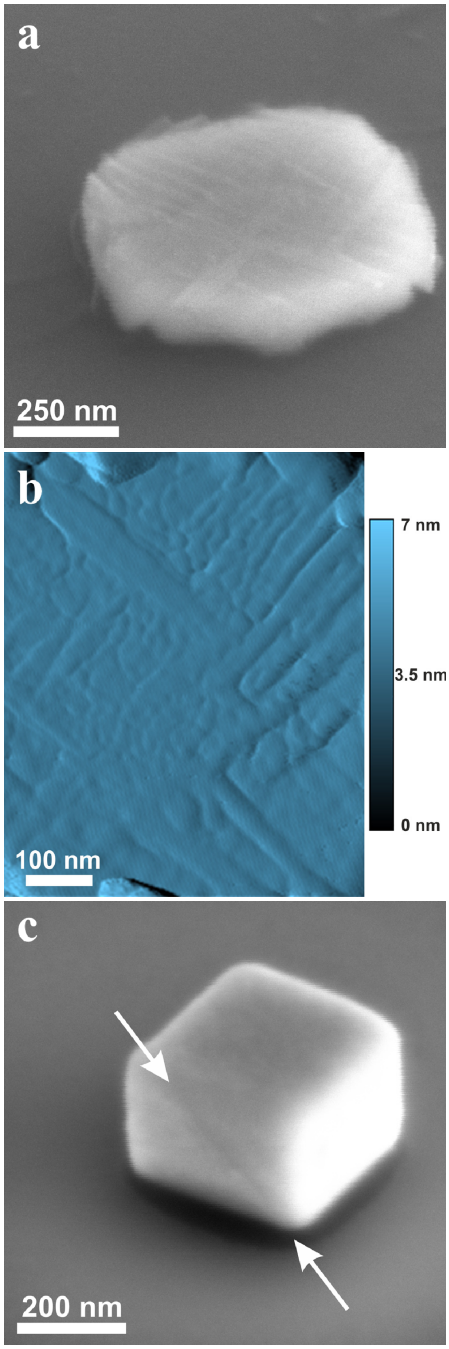

Figure 10: (a) A SEM image of the compressively deformed morphology of the electrolytically extracted γ' particle that appears to structurally collapse into a pancake shape. (b) An AFM tapping mode image of the deformed morphology of the electrolytically extracted γ' particle and numerous slip lines and terraces are visible. (c) A SEM image of the deformed morphology of ion-imaged γ' particle; only a few slip lines are resolved and their cubic shape is retained.

The large distribution of activation stresses in the ion-imaged γ' particles may be due to the statistical distribution of surface defects. In contrast to the numerous slip lines on the top surfaces of electrolytically extracted γ' particles, the top surfaces of ion-imaged γ' particles exhibit a negligible density of slip lines and remain flat. This characteristic behavior is similar to the deformation response of Au FCC microparticles [31] prepared without Ga^+ ion implantation. The observation that large strain burst is not present in the stress-displacement curve of ion-imaged γ' particles implies that mechanical annealing [27] did not occur. With the activation of plastic deformation at a stress that is significantly lower than the theoretical stress, mass nucleation and propagation of dislocations are very unlikely to occur in ion-imaged γ' particles.

As shown by Figure 9(a), a yield strength in excess of 10 GPa was measured via *in-situ* nano-compression of electrolytically extracted γ' particles, which is more than 5 GPa higher than the measured yield stress of ion-imaged γ' particles. This result is consistent with studies pertaining to the influence of Ga^+ ion implantation on the nano-mechanical response of nano- and micro-pillars [21,32-34]. For ion-imaged samples, Ga^+ ions may become implanted in the material or induce the formation of vacancies that condense to form dislocation loops. All of these defects contribute to lowering the strength of the dislocation-free γ' particles as they serve as potential sites for dislocation nucleation and multiplication at stresses significantly lower than those required for the homogeneous dislocation nucleation [35].

This reduced threshold stress of dislocation-free particles due to the ion beam milling can be approximated by $Gb/2\pi r_c$, with b being the Burgers vector and r_c being the critical radius for the nucleation of a stable dislocation loop. With a Burgers vector of 0.309 nm [36] and a typical pre-existing dislocation loop that is approximated with a circular diameter of 2 nm, the threshold stress required to expand the dislocation loop is 1.7 GPa, which is a factor of 4 lower than that required for the homogeneous dislocation nucleation. Newly formed dislocations tend to interact with these pre-existing defects and form locks, resulting in the strain hardening [37, 38]. This explains the observation that the cuboidal shape of the ion-imaged γ' particles is retained following deformation as the material responds to the steadily increasing stress by the intersection and multiplication of dislocations. The above analysis is consistent with other reported studies [20] and illustrates that the presence of pre-existing dislocations or surface defects may significantly decrease the observed yield strength.

Joint analysis of nanoindentation and nano-compression results

The measured hardness value of the γ' particles in the 'standard' CMSX-4 by nanoindentation is ~8.5 GPa. This result is consistent with other published nanoindentation results of CMSX-4 [24] and corresponds to a flow stress of 2.8 GPa when considering the standard relationship where $H=3*\sigma$ [39]. However, this flow stress is significantly lower than the maximum yield stress of electrolytically extracted, dislocation-free γ' particles, 10 GPa, measured via nano-compression testing. The difference in the magnitude of the flow stresses measured via nanoindentation and nano-compression tests is consistent with our explanation that the nanoindentation measurement results of the γ' particles tends to be affected by the surrounding softer γ matrix.

The measured hardness of the coarsened γ' particles of the 'coarsened' CMSX-4 (H=9.5 GPa and σ= 3.2 GPa) is also lower than the equivalent hardness estimated from the nano-compression tests (H=~30 GPa). For the coarsened γ' particles, although the plastic deformation of the surrounding γ matrix is minimized, the influence of the soft γ matrix on the system compliance may result in a lower measured hardness value.

Moreover, due to the difficulty of manufacturing atomically sharp indenters, the tip of the Berkovich indenter is typically rounded. As a result, prior to the 'pop-in' behavior, the deformation is purely elastic. For dislocation-free structures and crystals, when the shear stress under the tip reaches a value near their theoretical shear strength, dislocations will nucleate homogeneously. This is followed by subsequent glide and multiplication events that manifest itself as the occurrence of 'pop-in'. For materials containing dislocations and other crystal defects, however, stresses that are significantly lower than the theoretical stress are required to activate existing dislocation sources [40].

The reduced hardness value associated with the 'coarsened' γ' precipitates can likely be attributed to the presence of surface dislocations introduced by mechanical polishing or pre-existing dislocations and crystal defects formed during the coarsening heat treatment. Ongoing investigations are aimed at clarifying this discrepancy and developing robust measurement techniques capable of accurately assessing the nano-mechanical properties of the constituent γ and γ' phases in Ni-base superalloys.

Conclusions

Based on the nanoindentation measurement of the constituent phases of the 'standard' and 'coarsened' CMSX-4 and the nano-compression tests of as-extracted, dislocation-free γ' particles and ion-imaged γ' particles, the following conclusions can be drawn.

- Indentation response of the coarsened precipitates of CMSX-4 after a coarsening heat treatment was characterized using an AFM-based nanoindentation system and demonstrates the influence of the surrounding soft γ matrix on the measurement of nano-mechanical properties of the γ' particles.

- The measured hardness of the coarsened γ' precipitates in the 'coarsened' CMSX-4 appears to increase slightly with the increasing load.

- Yield strengths in excess of 10 GPa were measured via nano-compression testing of freestanding, dislocation-free γ' precipitates. These values, equivalent to ~G/17, are more than a factor of 33 higher than the testing results of their bulk counterparts.

- The strongest as-extracted, dislocation-free γ' particle exhibits yield stress more than 5 GPa higher than those ion-imaged γ' particles. This highlights the "softening" effect of Ga^+ ion implantation on the dislocation-free nanocrystals.

References

[1] R. Schafrik and R. Sprague, "Gas Turbine Materials Part II," Advanced Mater. & Processes, 162 (2004), 27–30.

[2] T.M. Pollock and S. Tin, "Nickel-based Superalloys for Advanced Turbine Engines: Chemistry, Microstructure, and Properties," J. Propulsion & Power, 22 (2006), 361.

[3] R.C. Reed, The Superalloys Fundamentals & Applications, (Cambridge University Press, 2006), p.1-2.

[4] T.M. Pollock and A.S. Argon, "Creep Resistance of CMSX-3 Nickel Base Superalloy Single Crystals," Acta Mater., 40 (1992), 1-3.

[5] E.P. Busso, F.T. Meissonnier and N.P. O'Dowd, "Gradient-Dependent Deformation of Two-phase Single Crystals," J. Mech. Phys. Solids, 48 (2000), 2333-2361.

[6] W.C. Oliver and G.M. Pharr, "An Improved Technique for Determining Hardness and Elastic Modulus Using Load and Displacement Sensing Indentation Experiments," J. of Mater. Res., 7 (1992), 1564.

[7] M.D. Uchic, P.A. Shade and D.M. Dimiduk, "Plasticity of Micrometer-Scale Single Crystals in Compression," Annu. Rev. Mater. Res., 39 (2009), 361.

[8] J.R. Greer and J.Th.M. De Hosson, "Plasticity in Small-sized Metallic Systems: Intrinsic versus Extrinsic Size Effect," Prog. of Mater. Sci., 56 (2011), 654-724.

[9] T.M. Pollock and R.D. Field, "Dislocations and High-temperature Plastic Deformation of Superalloy Single Crystals", Dislocations in Solids, (Elsevier Science B.V., 2002), p.554.

[10] M.D. Uchic, D.M. Dimiduk, J.N. Florando and W.D. Nix, "Sample Dimensions Influence Strength and Crystal Plasticity," Science, 305 (2004), 986.

[11] J.R. Greer, W.C. Oliver and W.D. Nix, "Size Dependence of Mechanical Properties of Gold at the Micron Scale in the Absence of Strain Gradients," Acta Mater., 53 (2005), 1821.

[12] K. Harris et al., "Development of the Rhenium Containing Superalloys CMSX-4 and CM186LC for Single Crystal Blade and Directionally Solidified Vane Applications in Advanced Turbine Engine," Superalloys, (TMS, Warrendale, PA, 1992), p. 301.

[13] R. Völkl, U. Glatzel and M. Feller-Kniepmeier, "Measurement of the Lattice Misfit in the Single Crystal Nickel Based Superalloys CMSX-4, SRR99 and SC16 by Convergent Beam Electron Diffraction," Acta Mater., 46 (1998), 4404.

[14] A.M. Minor, S.A.S. Asif, Z.W. Shan, E.A. Stach, E. Cyrankowski, T.J. Wyrobek and O.L. Warren, "A New View of the Onset of Plasticity during the Nanoindentation of Aluminium," Nature Mater., 5 (2006), 697.

[15] M. Feller-Kniepmeier and T. Link, "Dislocation Structures in γ-γ' interfaces of the Single Crystal Superalloy SRR99 after Annealing and High Temperature Creep," Mat. Sci. Eng. A, 113 (1989), 191-195.

[16] W.D. Nix and H.J. Gao, "Indentation Size Effects in Crystalline Materials: A Law for Strain Gradient Plasticity," J. Mech. Phys. Solids, 46 (1998), 411.

[17] T.Link, A. Epishin, U. Bruckner and P. Portella, "Increase of Misfit during Creep of Superalloys and Its Correlation with Deformation," Acta Mater., 48 (2000), 1981-1994.

[18] J. Schloesser, J. Rösler and D. Mukherji, "Deformation Behavior of Freestanding Single-Crystalline Ni_3Al-based Nano-particles," Int. J. Mat. Res., 102 (2011), 532-537.

[19] B. Gan and S. Tin, "*In-situ* Nano-compression testing of Freestanding γ' particles inside TEM," unpublished work.

[20] H. Bei, S. Shim, G.M. Pharr and E.P. George, "Effects of Pre-strain on the Compressive Stress-Strain Response of Mo-Alloy Single-Crystal Micro-Pillars," Acta Mater., 56 (2008), 4762-4770.

[21] S. Shim, H. Bei, M.K. Miller, G.M. Pharr and E.P. George, "Effects of Focused Ion Beam Milling on the Compressive Behavior of Directionally Solidified Micropillars and the Nanoindentation Response of An Electropolished Surface," Acta Mater., 57 (2009), 503-510.

[22] B. Bhushan and V.N. Koinkar, "Nanoindentation Hardness Measurements Using Atomic Force Microscopy," Appl. Phys. Lett., 64 (1994), 1653-1655.

[23] M. Göken and M. Kempf, "Microstructural Properties of Superalloys Investigated by Nanoindentations in An Atomic Force Microscope," Acta Mater., 47(1998), 1043-1052.

[24] K. Durst and M. Göken, "Micromechanical Characterization of the Influence of Rhenium on the Mechanical Properties in Nickel-base Superalloys," Mater. Sci. Eng. A, 387–389 (2004), 312–316.

[25] T. Schöberl, H.S. Gupta and P. Fratzl, "Measurements of Mechanical Properties in Ni-base Superalloys Using Nanoindentation and Atomic Force Microscopy," Mater. Sci. Eng. A, 363 (2003), 211–220.

[26] Z.J. Wang, Z.W. Shan, J. Li, J. Sun and E. Ma, "Pristine-to-Pristine Regime of Plastic Deformation in Submicron-Sized Single Crystal Gold Particles," Acta Mater., 60 (2012), 1368.

[27] Z.W. Shan, R.K. Mishra, S.A.S. Asif, O.L. Warren and A.M. Minor, "Mechanical Annealing and Source-limited Deformation in Submicrometer-diameter Ni Crystals," Nature Mater., 7 (2007), 115.

[28] S.S. Brenner, "Tensile Strength of Whiskers," J. of Appl. Phys., 27 (1956), 1484-1491.

[29] S.S. Brenner, "Plastic Deformation of Copper and Silver Whiskers," J. of Appl. Phys., 28 (1957), 1023-1026.

[30] G. Richter, K. Hillerich, D.S. Gianola, R. Mönig, O. Kraft and C.A. Volkert, "Ultrahigh Strength Single Crystalline Nanowhiskers Grown by Physical Vapor Deposition," Nano Lett., 9 (2009), 3048-3052.

[31] D. Mordehai, S.W. Lee, B. Backes, D.J. Srolovitz, W.D. Nix and E. Rabkin, "Size Effect in Compression of Single-Crystal Gold Microparticles," Acta Mater., 59 (2011), 5202-5215.

[32] D. Kiener, C. Motz, M. Rester, M. Jenko and G. Dehm, "FIB Damage of Cu and Possible Consequences for Miniaturized Mechanical Tests," Mater. Sci. Eng. A, 459 (2007), 262–272.

[33] H. Bei, S. Shim, M.K. Miller, G.M. Pharr and E.P. George, "Effects of Focused Ion Beam Milling on the Nanomechanical Behavior a Molybdenum-alloy Single Crystal," Appl. Phys. Lett., 91 (2007), 111915.

[34] R. Maaß, S. Van Petegem, C.N. Borca and H. Van Swygenhoven, "*In-situ* Laue Diffraction of Metallic Micropillars," Mater. Sci. Eng. A, 524 (2009), 40-45.

[35] C.R. Weinberger and W. Cai, "Surface-controlled Dislocation Multiplication in Metal Micropillars," PNAS, 105 (2008), 14304-14307.

[36] F.E. Heredia and D.P. Pope, "Effect of Boron Addition on the Ductility and Fracture Behavior of Ni_3Al Single Crystals," Acta Metall., 39 (1991), 2017-2026.

[37] C.R. Weinberger and W. Cai, "The Stability of Lomer-Cottrell Jogs in Nanopillars," Scripta Mater., 64 (2010), 529-532.

[38] A.T. Jennings, J. Li and J.R. Greer, "Emergence of Strain Rate Sensitivity in Cu Nano-Pillars: Transition from Dislocation Multiplication to Dislocation Nucleation," Acta Mater., 59 (2011), 5627-5637.

[39] D. Tabor, The Hardness of Metals, (Oxford University Press, 2000).

[40] A. Barnoush, M.T. Welsch and H. Vehoff, "Correlation between Dislocation Density and Pop-in Phenomenon in Aluminum Studied by Nanoindentation and Electron Channeling Contrast Imaging," Scripta Mater., 63 (2010), 465-468.